Research Article | Vol. 10, No. 4 | 1 Apr 2019 | BIOMEDICAL OPTICS EXPRESS 1841
Biomedical Optics EXPRESS

Hydration and nanomechanical changes in collagen fibrils bearing advanced glycation end-products

Orestis G. Andriotis,[1] Kareem Elsayad,[2] David E. Smart,[3] Mathis Nalbach,[1] Donna E. Davies,[3,4] and Philipp J. Thurner[1,*]

[1]*Insitute of Lightweight Design and Structural Biomechanics, TU Wien, Getreidemarkt 9, 1060 Vienna, Austria*
[2]*Advanced Microscopy Section, Vienna Biocenter Core Facilities GmbH, Dr. Bohr-Gasse 3, 1030 Vienna, Austria*
[3]*NIHR Southampton Biomedical Research Centre, Clinical and Experimental Sciences, Faculty of Medicine, University of Southampton, Southampton, United Kingdom*
[4]*Institute for Life Sciences, University of Southampton, Southampton, United Kingdom*
**pthurner@ilsb.tuwien.ac.at*

Abstract: Accumulation of advanced glycation end-products (AGEs) in biological tissues occurs as a consequence of normal ageing and pathology. Most biological tissues are composed of considerable amounts of collagen, with collagen fibrils being the most abundant form. Collagen fibrils are the smallest discernible structural elements of load-bearing tissues and as such, they are of high biomechanical importance. The low turnover of collagen cause AGEs to accumulate within the collagen fibrils with normal ageing as well as in pathologies. We hypothesized that collagen fibrils bearing AGEs have altered hydration and mechanical properties. To this end, we employed atomic force and Brillouin light scattering microscopy to measure the extent of hydration as well as the transverse elastic properties of collagen fibrils treated with ribose. We find that hydration is different in collagen fibrils bearing AGEs and this is directly related to their mechanical properties. Collagen fibrils treated with ribose showed increased hydration levels and decreased transverse stiffness compared to controlled samples. Our results show that BLS and AFM yield complementary evidence on the effect of hydration on the nanomechanical properties of collagen fibrils.

1. Introduction

Modern diet in western societies is largely enriched in sugars causing increasing levels of obesity and diabetes. This is evidenced by the rapidly increasing sugar consumption per capita, which is comparable to the increasing obesity rates [1] and the number of people diagnosed with diabetes [2]. As a secondary consequence, advanced glycation end-products (AGEs) accumulate in biological tissues [3,4], and, have been associated with the impairment of tissue functionality such as cell adhesion [5] and wound healing [6]. AGEs contribute to long term complications such as nephropathy [7] or retinopathy [8] as well as connective tissue disorders such as Alzheimer's disease [9], atherosclerosis [10,11] and osteoporosis [12] i.e. age-related increase of fracture risk of bones. One major implication of diabetes is the impairment of mechanical properties of connective tissue [13], and, such mechanical implications have been associated to the glycation of collagen [14–16]; the major structural and mechanically functional element of the extracellular matrix (ECM) of biological tissues.

Glycation is the reaction of a sugar with an amino acid, via the well-known Maillard reaction [17]. Specifically, the aldehyde or ketone group of a reducing sugar reacts with the free amino group of an amino acid. This process forms AGE adducts. In collagens, the AGE adducts are formed on lysine residues. A glycated lysine can further react with a lysine or arginine forming an AGE cross-link either intra- or intermolecularly. Collagens, due to their

#355186 https://doi.org/10.1364/BOE.10.001841
Journal © 2019 Received 12 Dec 2018; revised 20 Feb 2019; accepted 20 Feb 2019; published 14 Mar 2019

Biomedical Optics EXPRESS

high abundance (approx. 1/3 of protein mass in human body) and low turnover [18], are highly susceptible to glycation. Because collagen turnover is reduced with age [19], AGEs accumulate in healthy elderly individuals [20], such that glycation of collagen becomes more prevalent with increasing age.

Collagens provide tissues with varying mechanical properties [21]. Given the hierarchical architecture of biological tissues, one needs to consider the composition, structure and chemical modifications of collagen to understand how the varying mechanical properties are achieved. Collagen molecules are characterized by the tight folding of three alpha-chains into a triple helix, achieved by the high abundance of Gly residues at every third position along each alpha-chain [22]. The triple helical structure of collagen molecules is characterized as an uninterrupted sequence of more than 300 Gly-X-Y motifs that are flanked by short non-helical domains, the telopepetides. A number of different collagen types exist, but the most abundant are the fibril-forming collagens. Fibril-forming collagen molecules can spontaneously self-assemble (fibrillogenesis) into a super-molecular structure; the collagen fibril. Collagen fibrils are rope-like structures with lengths up to 1 cm [23] and, depending on the age and type of tissue, with diameters ranging from 10 nm to more than 500 nm [24]. Collagen fibrils are the most abundant and smallest structural elements discernible with microscopic imaging techniques, such as scanning electron and atomic force microscopy, and are considered to be the basic building blocks of collagen-rich tissues with great biomechanical importance. Tissue mechanics at the microscale and nanoscale have been investigated by means of contact and non-contact methods. Atomic force microscopy (AFM) provides a contact method for mechanical assessment of biological tissues down to the nanoscale of individual collagen fibrils [25–31]. On the other hand, Brillouin light scattering (BLS) has been proposed as a reliable non-contact method for testing tissue mechanics at the sub-cellular level [32], as well as the dynamics of water molecules in biological tissues [33–36]. In fact, AFM and BLS have yielded comparable results [32,37]. Considering, the hierarchical architecture of biological tissues and the volume assessed via AFM and BLS, these two techniques could be used in a complementary fashion.

In physiology, collagen fibrils are highly hydrated. Atomic force microscopy experiments have shown that the volume of collagen fibrils increases up to 5-fold upon hydration [25,26,28,29]. In a volumetric sense, the hydrated collagen fibril contains more water than collagen ground substance. Hydration is therefore an important factor affecting collagen fibril mechanics [38], presumably through changes in the density of noncovalent interactions, measured directly at the collagen fibril level under tension [26] and indentation-type loading [28,29]. Indentation-type AFM loading revealed a three to four orders of magnitude difference between the indentation modulus of hydrated and air-dried collagen fibrils [25]. BLS has also illustrated changes in the resulting spectra upon dehydration of collagen [34–36] and muscle [36]. One can therefore employ BLS in biological tissues to study the dynamics of water molecules in a material or sample of interest.

Beyond hydration, the biochemistry of collagen fibrils also plays an important role in the structural stability of collagen fibrils. Collagen fibrils are formed due to hydrophobic interactions between collagen molecules and the fibrillar structure is further stabilized by enzymatically-mediated covalent cross-links (through the copper-dependent lysyl oxidase enzyme family) of the short non-helical domains [3]. AGEs are the type of cross-links in collagen fibrils that are formed non-enzymatically i.e. sugar-mediated.

Generally, accumulation of AGE cross-links increases tissue stiffness measured at the macroscale. Accumulation of AGE cross-links involve a number of intermediate steps. Before the formation of an intermolecular cross-link, the reaction of a reducing sugar with an amino acid initially results in the stable formation of AGE adducts. AGE adducts bear hydrogen bond donors and acceptors that adsorb water molecules. It may well be, that during the formation of AGE adducts more water is adsorbed within the collagen fibrils. However, the potential effect of AGE adducts on the hydration level, and therefore mechanical properties,

Biomedical Optics EXPRESS

of collagen fibrils is not well understood. We hypothesized that hydration of collagen fibrils is, to some extent, influenced by the chemical alterations from the formation of AGE adducts and/or cross-links. To test this hypothesis, we treated collagen samples from a mouse tail tendon with ribose. Ribose is a pentose, the reaction of which with the amino group of lysine and arginine results in the formation of pentosidine; a naturally occurring AGE in collagen fibrils. We then assessed the hydration and mechanical properties of collagen samples by employing both Brillouin light scattering and atomic force microscopy experiments.

2. Materials and methods

2.1 In vitro glycation of collagen fibrils

Collagen fibril samples: A tendon fascicle, collected from the tail tendons of a two-month-old mouse, was cut in half. One-half was used as the control group and immediately deposited on a glass slide. To expose individual collagen fibrils, the fascicles were placed on poly-l-lysine coated glass slides and separated using the sharp apex of tweezers, using a previously published method [27]. The samples were washed in distilled water and then air-dried until further use. The other half of the tendon fascicle was separated into collagen strands and then incubated into a ribose solution to induce sugar-mediated glycation.

Glycation of collagen: Collagen strands were placed in Hank's Balanced Salt Solution (HBSS) containing 30mM HEPES (pH7.4), 0.6M ribose, to induce sugar-mediated glycation in collagen, and a broad spectrum of protease inhibitor cocktail. The samples were incubated in 37°C with the solution and protease inhibitors replaced every day. The glycated samples were harvested after 48 hours of incubation. Similarly, to the control group, the samples were washed with distilled water, deposited onto poly-l-lysine glass slides to expose individual collagen fibrils. The samples were air-dried until further use.

2.2 Atomic force microscopy

Instrumentation: Atomic force microscopy (AFM) experiments were conducted in a NanoWizard ULTRA SpeedA AFM (JPK Instruments AG, Berlin) instrument equipped with an inverted optical microscope (Axio Observer.D1, ZEISS). AFM imaging and cantilever-based nanoindentation were performed with rectangular silicon nitride cantilevers with a gold-coated backside (PNP-DB, 0.48 N/m nominal spring constant and backside gold-coated) equipped with a sharp pyrex nitride tip (3.5 μm nominal height and <10 nm tip radius). Prior to AFM scanning the spring constant of the cantilever was calibrated using the thermal noise method [39].

Imaging: AFM scans in air were conducted in contact mode. Initially, a scan was conducted in a region (20 μm x 20 μm; 512 x 512 pixel resolution; 1 Hz line rate; 1.5 nN setpoint) such that at least three individual collagen fibrils are visible and isolated from each other (Fig. 1). Then, three collagen fibrils were selected and individually scanned such that their long axis is aligned along the slow scan axis by adjusting the scan angle. This is favorable for automatization of post-processing and data analysis with the custom Matlab script (MATLAB 8.5 R2015b, The MathWorks Inc., Natick, MA). Individual collagen fibrils were scanned in air at 2.5 nN setpoint, 10 Hz line rate, 1.5 μm x 8 μm (fast x slow) scan size and 512 x 2730 pixel resolution. Subsequently, collagen fibrils were fully submerged in phosphate buffered saline (PBS, 10mM, pH7.4) and left for approximately 1 hour until thermal equilibrium prior to nanomechanical assessment via AFM.

Nanomechanical assessment via indentation-type AFM: The inverse optical lever sensitivity was calibrated in the aqueous solution, prior to mechanical testing the collagen fibrils. With the collagen fibrils fully submerged in the aqueous solution, an overview image in air was recorded in QI™ mode (Quantitative Imaging™, JPK Instruments); a fast version of force volume mapping (FVM). FVM allows to spatially resolve the nanomechanical properties over a region of interest by performing point-by-point force-indentation curves

Biomedical Optics EXPRESS

[40]. From every force-indentation curve, the z-piezo displacement at the contact point i.e. at zero force, provides a height topography image (Fig. 1). The height topography from the QI™ overview scan was used to collocate the hydrated collagen fibrils. Subsequently, indentation-type AFM nanoindentation was employed to mechanically assess the individual collagen fibrils via FVM, similarly to a previous study [27]. The region of the collagen fibrils scanned in air was selected to perform the FVM at 1.5 µm x 8 µm scan size and 40 x 54 pixel resolution (Fig. 1). Every pixel corresponds to a force-indentation curve (Fig. 1), i.e. 2160 such curves, from which 54 were recorded at the crest of the collagen fibril. Similarly, the FVM was recorded by aligning the long axis of the fibril along the slow axis of the scan. This simplifies our post-processing methodology for acquiring the height of the collagen fibrils as well as the force-indentation curves recorded at the crest of the fibril. As discussed previously, due to the cylindrical geometry of the collagen fibrils, its crest is regarded as a valid contact point between the AFM tip and the collagen fibril to measure mechanical properties [27].

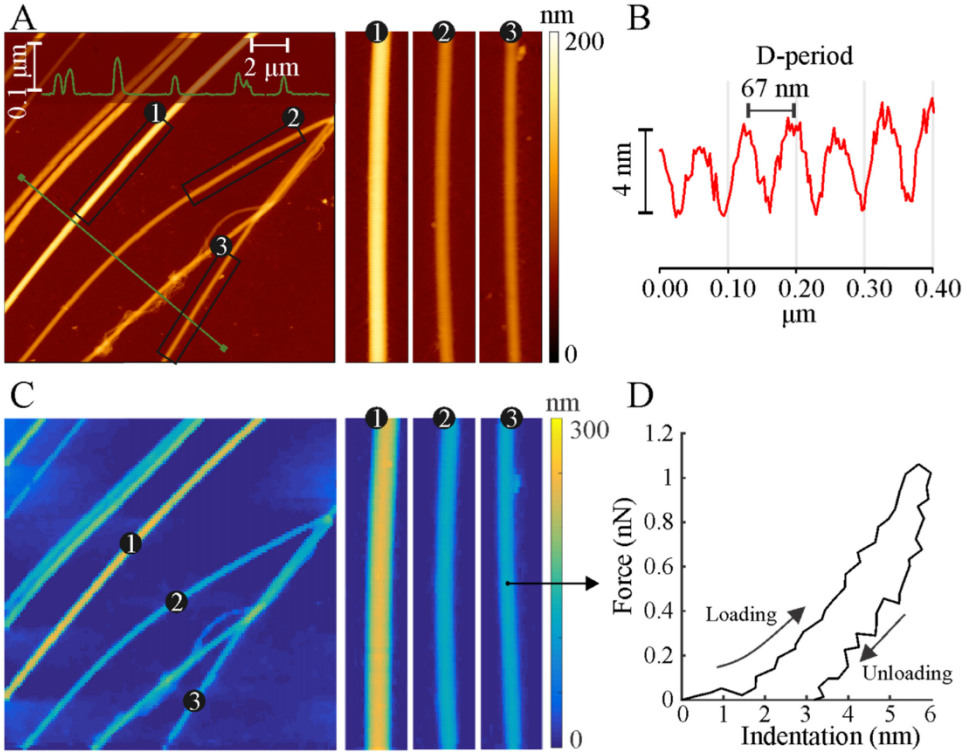

Fig. 1. (**A**). Overview height topography scan of collagen fibrils on a glass slide showing a cross-section profile (inset, scale bars correspond to inset only) and examples of the selected collagen fibrils (rectangles, A). (**A, 1-3**) AFM height topography scans in air of the three selected collagen fibrils. (**B**). Characteristic D-periodicity with which collagen fibrils are distinguishable from other proteins. (**C**). The overview scan in PBS and (**C, 1-3**) the force volume maps of the individual collagen fibrils. (**D**). Characteristic force-indentation curve from the crest of the collagen fibril. In both air and PBS, the scan size of the overview images was 20 µm x 20 µm and that of the individual collagen fibrils was 1.5 µm x 8 µm.

Fibril height measurements and swelling: The height topography images of the collagen fibrils, were used to determine the height of the collagen fibrils in air and PBS. As shown in Fig. 2, the collagen fibril height was estimated to be the difference between the maximum point of every scan line (54 in total per collagen fibril) and the average height of the glass slide. The average height was calculated from these 54 measurements. The fold-

Biomedical Optics EXPRESS

increase in collagen fibril height from air to PBS was defined as the swelling of the collagen fibril upon hydration. In addition, the position of the maximum height within the FVM (indicated with red points located along the crest of the fibril in Fig. 2) were used to locate the 54 force-indentation curves for further analysis and calculation of the indentation modulus.

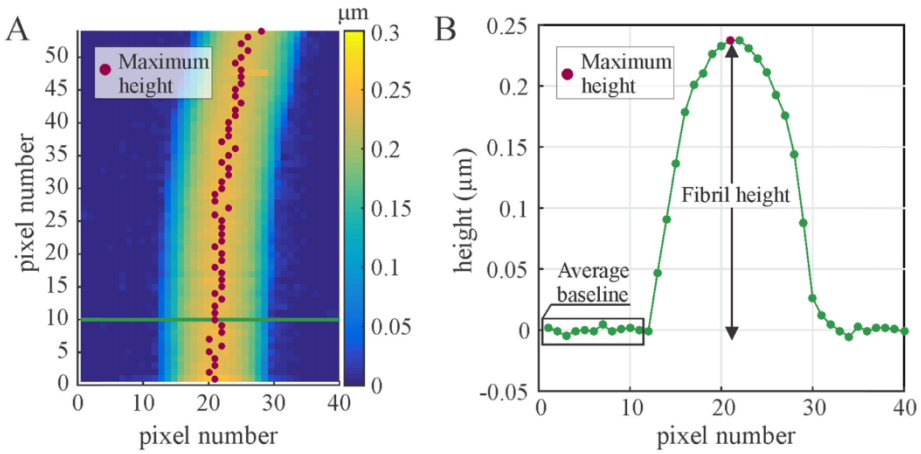

Fig. 2. Fibril height measurements from the height channel of the atomic force microscopy image or force-volume map. **A.** Height topography from the force-volume map constructed at contact point (zero force). The highest points, i.e. the crest of the collagen fibril, are highlighted with red points. The green line across the collagen fibril indicates the location selected as an example cross-section shown in (B). **B.** Line profile showing the estimation of fibril height. The fibril height was defined as the difference between the average baseline height and the maximum height (indicated with a red point) per line profile. The average height of the collagen fibril shown in A was 238.2 ± 5.2 nm (average ± standard deviation).

Indentation modulus calculation: The indentation modulus was estimated by implementing the Oliver-Pharr method [41], as previously described [27]. The indentation modulus of the sample, E_{sample}, is given by the equation:

$$E_{sample} = \beta \frac{\sqrt{\pi}}{2}\left(1-\nu^2\right)\frac{S_C}{\sqrt{A_c}} \quad (1)$$

where $\nu = 0.5$ is the Poisson's ratio of collagen [28,31], S_C is the contact stiffness and A_C the projected area of contact between the tip and the sample at the contact depth h_C. The contact stiffness, S_C, is the slope of the upper unloading part of the force-indentation curve corrected by that taken on the glass slide. To estimate the projected area of contact, a TGT1 calibration grating was imaged. Briefly, a sharp spike of conical shape (5 nm tip radius, 50 degrees opening angle) from the calibration grating (TGT1, NT-DMT) was imaged in contact mode over a 1.5 μm x 1.5 μm scan region at 512 x 512 pixel resolution. The resulting enveloped height topography data between the tip and the spike were corrected by the known TGT1 spike 3D geometry providing the height data of the AFM tip [42]. This method of determining the projected area of contact has been previously validated by comparison with conventional nanoindentation on polymers yielding comparable results [27]. The AFM tip height data where then used to provide the projected area function, A_C.

2.3 Brillouin light scattering

Brillouin light scattering. Spontaneous Brillouin Light Scattering (BLS) spectroscopy measures the inelastic scattering of light from inherent thermal density fluctuations - acoustic phonons – in a sample [43]. In the back-scattering geometry light couples to the longitudinal acoustic phonon mode resulting in a single scattering peak for an effectively homogeneous

Biomedical Optics EXPRESS

probing volume, the position of which relative to the probing laser frequency is directly proportional to the hypersonic velocity of the longitudinal acoustic phonons. This is in turn proportional to the square root of the longitudinal storage modulus (M') at the probed frequency, via the Cristoffel equation. The inherent width of the peak due to homogeneous broadening on the other hand is related to the lifetime of the probed acoustic phonons and can be shown to be proportional to the longitudinal loss modulus (M") and effective viscosity. By using a high Numerical Aperture (NA) objective lens it is possible to effectively probe a sample from different directions resulting in several distinct scattering peaks in a mechanically anisotropic sample.

To obtain a value for the longitudinal elastic storage modulus (M ') from the BLS frequency shift (w_B), knowledge of n^2/r, where r is the density and n is the refractive index, is required. In particular: $M' \sim C\,(r / n^2)\, w_B^2$, where C is a numerical constant depending on the scattering geometry and probing wavelength. Since the exact value of r and n are not known during the course of dehydration, we quote all results only as the BLS frequency shift. We note that according to the Lorentz-Lorenz relation, this ratio can to a first approximation be assumed constant, and that the percentage change in either of the individual parameters as well as their ratio is expected to be much smaller than that of the observed BLS frequency shift. As such, one would expect the longitudinal elastic storage modulus will scale approximately as the square of the BLS frequency shift.

The derived elastic modulus measured by BLS differs from that measured using AFM in several critical ways and should be seen as providing complimentary information rather than as a comparable measurement. Firstly, the BLS-measured M' is a measure of the relative strain along the axis corresponding to the phonon wavevector that is being scattered from, that would result from an applied pressure along this same axis under the constraint of no lateral extension. The indentation modulus probed using AFM, while also effectively measuring the relative strain in the probing direction subject to a given force, does not have this constraint on lateral extension, and as such, incompressible materials will have a much lower modulus. Furthermore, while AFM by design requires the sample to be physically perturbed by a measurable amount, BLS does not impose any physical perturbation. Since water is essentially incompressible, hydration of a sample can have a strong influence on the measured BLS modulus, and indeed BLS can be used to assess the level of hydration of samples [34–36].

Secondly, the length scales probed with BLS will depend on the characteristic length scales of the acoustic phonons at the probed frequencies. Namely, when probing at visible wavelengths the effective probed acoustic wavelength will be on the order of 200 nm, while the attenuation length of the acoustic modes can be a few micrometers depending on the rigidity of the material. If a sample has heterogeneities only much smaller than these characteristic length scales then it may to a first approximation be treated as an effective medium, giving rise to a single Brillouin Scattering peak for a given phonon wavevector. In the event of sample heterogeneities on scales larger than the characteristic acoustic scale yet smaller than the probed volume (effective excitation-detection point spread function) the measured spectrum will however consist of a weighted superposition of the constituent spectra in the enclosed probing volume. Thus, unlike AFM, the effective length scales for which mechanical properties are measured depends on the characteristic scales of the acoustic waves being probed as well as the excitation-detection point spread function (scattering volume) which is defined by the effective numerical aperture of the objective lens. While the characteristic length scales of the derived mechanical properties are the former (namely the acoustic wavelength and attenuation length of the phonons), depending on the relative dimensions of the latter one may measure a spatial and orientational average in the probed volume [44,45].

Finally, since the frequency of the acoustic phonons probed is on the order of several GHz, the mechanical response is also being measured at these frequencies. All biological

Biomedical Optics EXPRESS

materials are more or less viscoelastic, and at these high frequencies, they are generally at or beyond the glass transition. The BLS derived elastic moduli are thus typically orders of magnitude larger than those obtained using quasi-static techniques.

Experimental Setup. The experimental setup employed consists of a confocal sample scanning microscope with a physical (100 μm) pinhole, coupled to a Virtual Imaged Phase Array (VIPA) cross-dispersion spectrometer originally proposed by Scarcelli and Yun [46]. Excitation was via a 532 nm single frequency laser (Torus, Laser Quantum), with the typical excitation powers at the sample being 1-3 mW. Images were acquired using a 1.42NA 60x immersion objective (Olympus APO), with an effective excitation-detection point-spread-function Full-Width-at-Half-Maximum (FWHM) of 260 nm laterally and 520 nm axially. The setup allowed for parallel widefield phase contrast imaging to locate regions of interest and monitor the sample during acquisition. A sketch of the microscope/spectroscope setup is shown in Fig. 3 (a more detailed description can be found in [47]). An example spatial map of the average frequency shift when scanning (control) fibers is shown in Fig. 4 . Typically, acquisition times where 100-200 ms per spectra, and scan steps in the Brillouin maps are typically 100 nm or as indicated by the pixel sizes in the plots. Prior and after each measurement calibration measurements on water and spectroscopic grade ethanol were performed for calibration and to assure system had not drifted during measurements. Least squares fitting of a Lorentzian function for the peaks was performed using a custom Matlab (Mathworks, Germany) script. All measurements were performed at ambient room temperature (25°C), which was continuously monitored during experiments and stable to within ± 0.5°C.

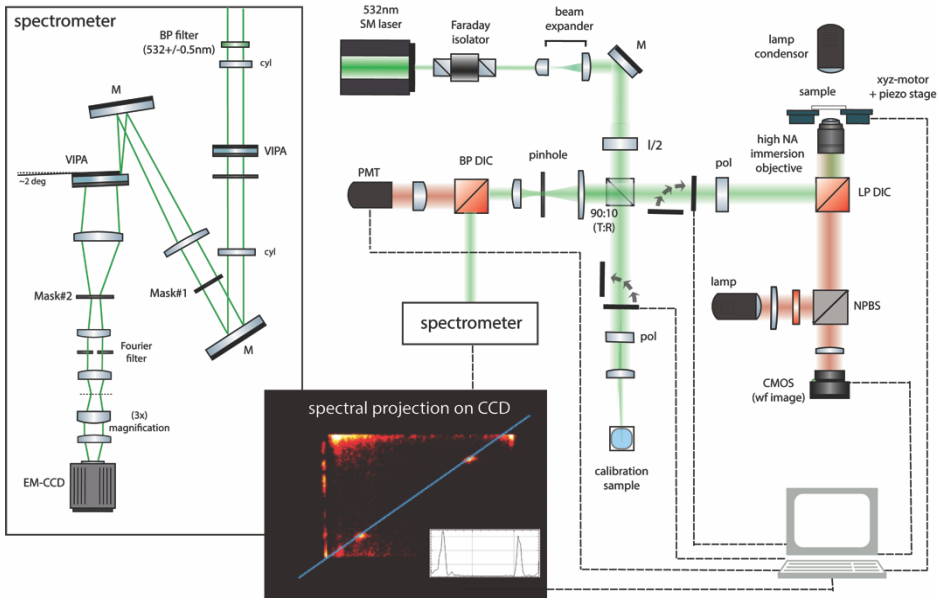

Fig. 3. Sketch of the microscope setup used for BLS measurements. Inset shows an example of the projected BLS spectra as measured on the EM CCD camera.

Biomedical Optics EXPRESS

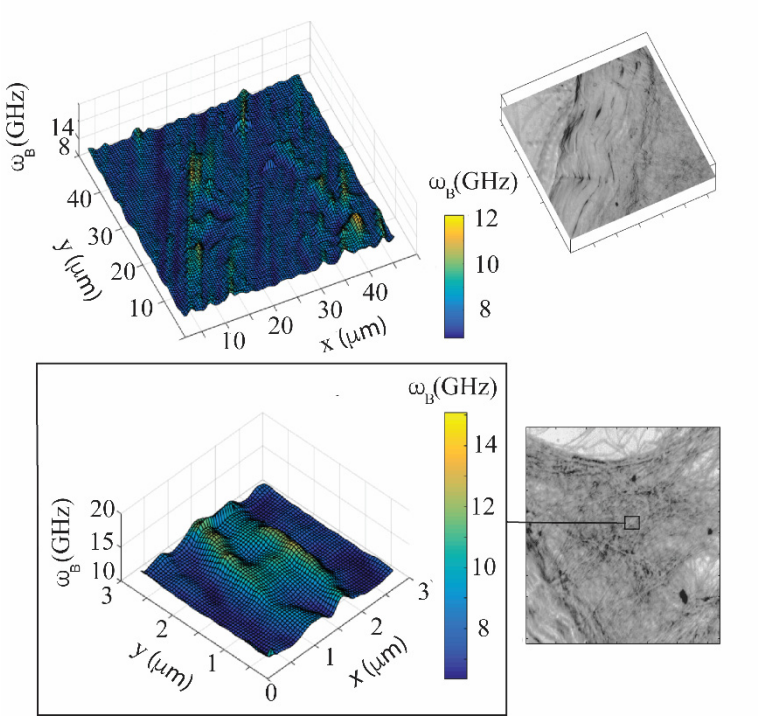

Fig. 4. Spatial maps of ω_B and corresponding widefield transmitted light images. (Field of view for widefield images is 45 μm x 45 μm).

3. Experimental results and discussion

Swelling, hydration and nanomechanics of ribose-treated collagen fibrils: In air, the average collagen fibril height was 100.8 ± 39.5 nm (n = 3 fibrils) and 106.5 ± 9.9 nm (n = 3 fibrils) from the control and ribose-treated samples, respectively. When the same fibrils were hydrated and measured in PBS, their average height was increased to 160.2 ± 55.0 nm for the control and 200.4 ± 10.4 nm for the ribose-treated samples. That is, upon hydration the control collagen fibrils swelled by (1.6 ± 0.1) times whereas the ribose-treated ones by (1.9 ± 0.1) times (Fig. 5). Previous studies have tested collagen fibrils from various sources, nevertheless, the hydration of collagen fibrils results to a similar extent of increase in fibril height (ranging from 1.5 to 2.6-fold change) [25,26,28,29].

Biomedical Optics EXPRESS

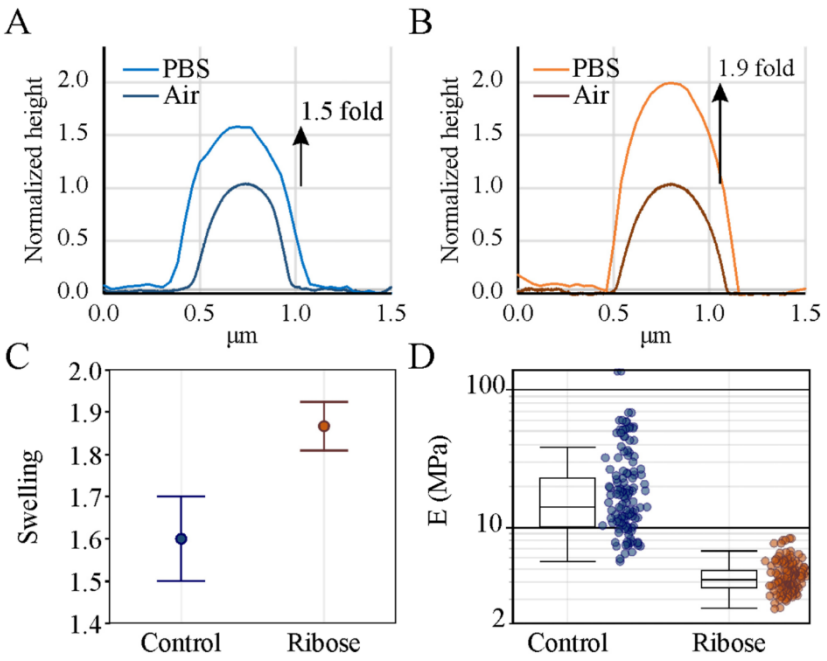

Fig. 5. A. and B. Normalized height profiles to the maximum height in air from a control and ribose-treated collagen fibril, respectively. C. Swelling, i.e. fold-increase in collagen fibril height, for control and ribose-treated. D. Indentation modulus values from control and ribose-treated collagen fibrils.

The Brillouin Light Scattering spectrum showed two peaks corresponding to phonons parallel and transverse to the fiber axis. The Brillouin spectra as extracted from the spectrometer were re-scaled according to the spectra obtained from distilled water and methanol measured at the time of imaging as described elsewhere [47]. The spectra were deconvolved by an experimentally measured spectral function obtained by measuring the Rayleigh peak with open slits at lower illumination intensity on the respective samples. This was assumed to be a good estimate of the complete instrumental spectral response as well as any broadening non-intrinsic to Brillouin scattering. Spectra were fitted using a Matlab function PeakFit based on a least-squares fitting algorithm with 4 Lorentzian functions (two Stokes and two anti-Stokes Brillouin peaks). In addition to the 4 independent Lorentzian functions a linear background term was included in the fit. From this the frequency shift and peak width of the two Brillouin peaks could readily be obtained. A characteristic fit for a the two (Stokes) peaks is shown in Fig. 6.

Biomedical Optics EXPRESS

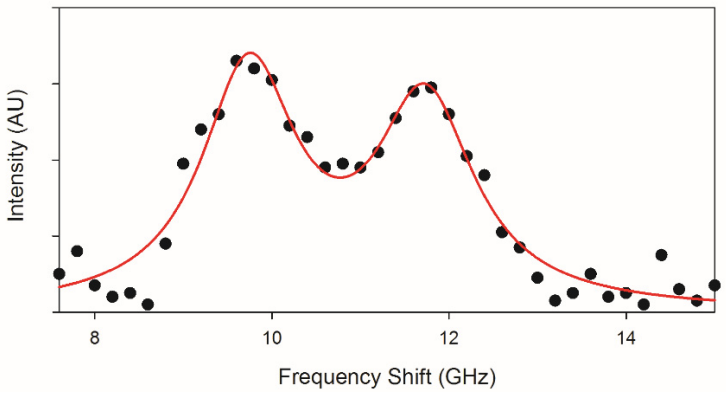

Fig. 6. Characteristic least-squares data fit for tokes Peaks of ribose treated sample.

At lower Numerical Aperture (NA) only a single (perpendicular to fiber axis) mode is observed in this imaging geometry but because of the very high NA a contribution from both components is present (Fig. 7(A)). In both control and ribose-treated samples, the peak position increased with dehydration, corresponding to an increase in "stiffness" (Fig. 7(B)). This is expected from past studies on dehydration of collagen fibers [33,34]. While the values of the lower frequency peak are in agreement with those previously measured for collagen, the higher frequency peak is at a slightly lower frequency as previously reported [33], which may be attributed to different sample preparation and/or the animal origins of the collagen. Interestingly, for the case of the ribose-treated collagen fibrils, the higher frequency peak (corresponding to the perpendicular to fibril axis phonon modes) showed a significantly decreased shift compared to the control samples when hydrated (~9 GHz compared to >10.5 GHz). The lower frequency peak on the other hand (corresponding to phonon modes parallel to the fibril axis) showed no such difference. During dehydration of the samples, the average value of the higher frequency peaks of the ribose-treated and control collagen fibrils appear to approach a common value (~12 GHz) (Fig. 8) and the lower frequency peaks both increased to ~9 GHz. The corrected width of the higher-frequency peak, related to the loss moduli and effective viscosity, was always approximately 20% larger for the ribose-treated collagen fibrils compared to the control ones, and both decreased by approximately 20-30% during the course of dehydration (inset of Fig. 8(A)). This observed trend may qualitatively be interpreted if one considers the frequency scaling of the elastic moduli. While the storage modulus can be assumed to increase with frequency, the storage and loss modulus in the vicinity of a glass transition are also expected to follow a Kramers-Kronig-type relation. A maximum in the loss modulus would thus occur at a glass transition. In a simplified case of a single or dominant phase transition one may assume the Loss Modulus decreases monotonically to higher and lower frequencies in the vicinity of such a transition. Above this transition one could thus expect an increase in the storage modulus (related to the frequency shift of the Brillouin peak) to coincide with a decrease in the loss modulus (related to the width of Brillouin peak) under the assumption that the nature of the transition has not been otherwise significantly perturbed. While at higher frequencies this trend is expected to break down, the results for our particular samples suggest we are in such an intermediate viscoelastic regime [48].

Biomedical Optics EXPRESS

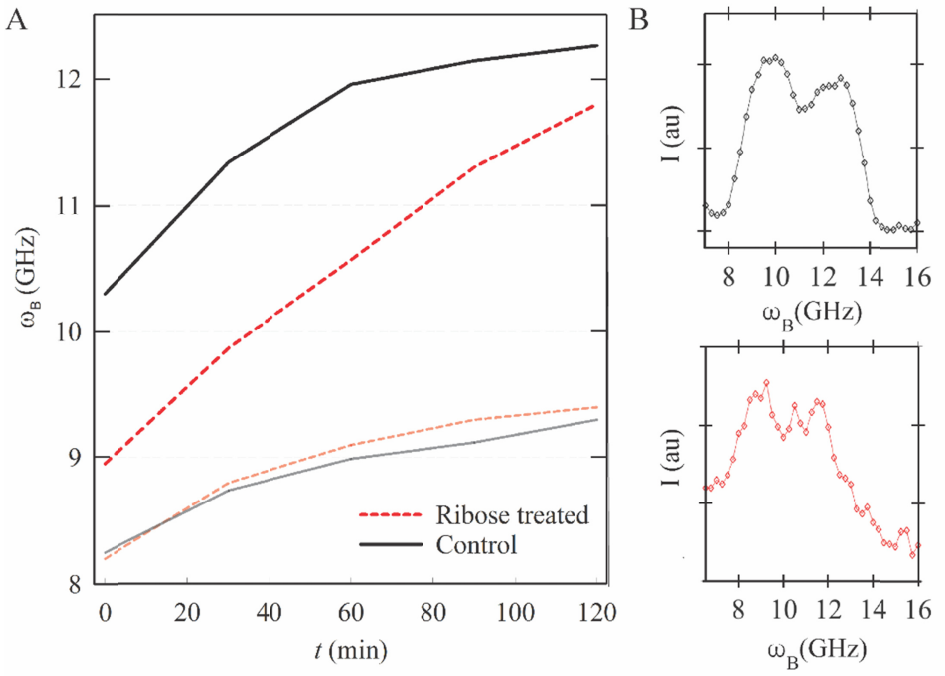

Fig. 7. (**A**): Plot of average frequency shift (ω_B) for the two observed Brillouin scattering peaks in control (black solid-line) and ribose-treated (red, dashed-line) collagen fibrils during dehydration. **B.** Example Brillouin light spectra at 120 min of dehydration for the control (top, black) and ribose-treated collagen fibrils (bottom, red).

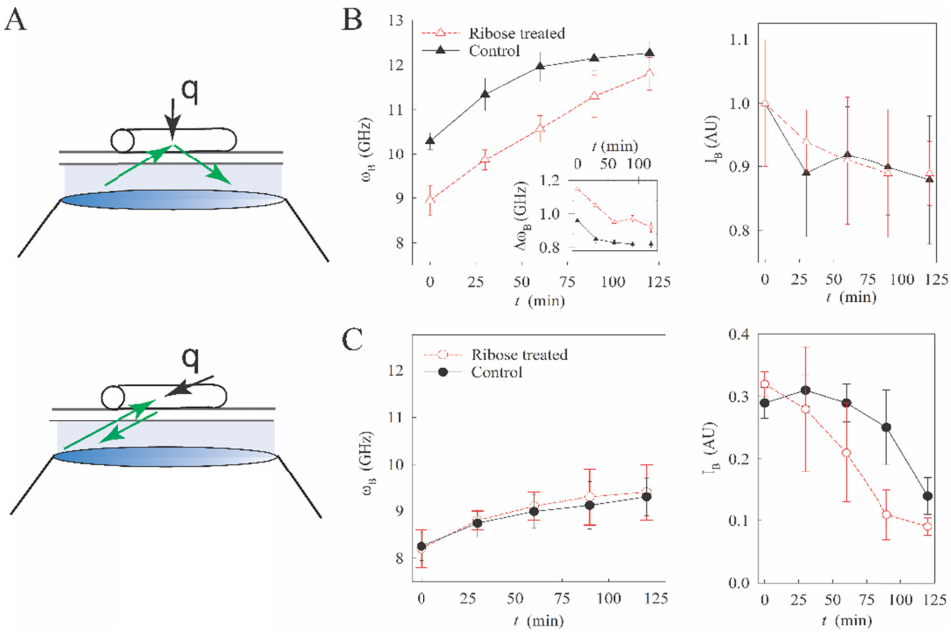

Fig. 8. (**A**): Sketch showing two different phonon wavevectors that can be coupled to with high NA objective. (**B**) [left]: BLS frequency shift ω_B of the higher frequency peak during dehydration (inset: corrected FHWM of peak after deconvolution). [Right]: Corresponding change in the relative peak intensity, I_B. (**C**): Same as (**A**), but for the lower frequency peak.

Biomedical Optics EXPRESS

Nanomechanical assessment via indentation-type AFM revealed the indentation modulus to be 19.9 ± 2.4 MPa (n = 3) for control samples versus the 4.4 ± 0.5 MPa (n = 3) for ribose-treated ones. Although the indentation modulus calculations may vary between different analytical models, the values presented here for hydrated collagen fibrils is within the MPa range, and similar values have been reported in previous studies [25,26,28–30]. Our results show that the indentation modulus of the control collagen fibrils is 78% higher compared to ribose-treated ones. The difference in swelling, can explain this difference to a large extent.

Ribose-treated collagen fibrils adsorb more water: The triple helical structure of collagen molecules is known to be stabilized through intramolecular peptide-peptide and peptide-water hydrogen bonds [49,50]. Here the structural water is tightly bound to the carboxyl groups, amide groups and polar amino acid side chains of collagen molecules [49,50]. In addition to bound water, water molecules can be adsorbed on collagen molecules through weak van der Waals (vdW) forces when, for example, collagen fibrils are suspended in an aqueous solution [51]. The adsorbed water molecules constitute the unbound water in collagen fibrils. Water molecules have high dielectric constant which reduces the free energy between collagen molecules within the fibrils [52]. Increasing content of unbound water, results in an increase of the intermolecular distance [53,54], which explains the swelling of hydrated collagen fibrils.

Changes in collagen fibril hydration are related to their nanomechanical properties [26]. Indentation-type AFM nanomechanical assessment employs a sharp tip (with a tip radius of approx. 10 nm) that indents the surface of the collagen fibril. The resulting loading is highly influenced by the packing density of the collagen molecules. The higher the packing density the higher is the indentation modulus. The indentation modulus of air-dried collagen fibrils is in the range of 1-10 GPa [25,27,28,31,55]. Upon hydration, the collagen fibril packing density decreases substantially, which explains the dramatic drop of the indentation modulus of about three orders of magnitude.

Collagen fibrils treated with ribose show higher swelling (1.9-fold) compared to control ones (1.6-fold). This can be explained by a higher amount of adsorbed (unbound) water from the ribose-treated collagen fibrils compared to control ones. The amount of water content within the fibril, i.e. the unbound water, has been related to changes in the equatorial spacing distance measured by X-ray diffraction [53,54]. The equatorial spacing distance is directly related to the intermolecular distance, and, therefore, the more unbound water adsorbed within the fibril the larger the intermolecular distance becomes [54]. Consequently, the intermolecular distance is increased and the molecular packing density is decreased in the ribose-treated samples. These structural changes at the fibril level of collagen are reflected by the 78% lower indentation modulus of the ribose-treated samples compared to the control ones.

Cross-link state may influence the hydration level: To understand the origin of hydration in collagen fibrils and the differences between control and ribose-treated samples in this study, we consider the biochemistry of collagen molecules and their dynamic interaction with water molecules. Collagen molecules bear many hydrogen bond donors and acceptors, which would result in hydration of the fibril at the early stages of fibrillogenesis.

During fibrillogenesis and throughout the lifetime of collagen fibrils, cross-links between or within collagen molecules are formed. Depending upon the formation process, two types of cross-links in collagen fibrils have been identified; a) the enzymatic and b) the non-enzymatic or sugar-mediated cross-links. In the former, the lysyl oxidase enzyme family initiates the cross-links at the early stages of fibrillogenesis. However, the sugar-mediated cross-links result from the non-enzymatic reaction between the amino group of an amino acid to the ketone group of a reducing sugar. AGE adducts are the initial stable products of the reaction between a reducing sugar and an amino group. With time, and, if stereochemically allowed, the AGE adduct will form a cross-link to a neighboring collagen molecule within the fibril. But, it is currently not known how much time is needed for the transition from an AGE

Biomedical Optics EXPRESS

adduct to a cross-link to occur. Therefore, we do not know which AGE products i.e. adducts or cross-links are prevalent after 48 hours of ribose treatment.

The characteristic of reducing sugars is the hydrogen bond donor and acceptor sites. These sites are solvated with water molecules and can hence increase the number of water molecules adsorbed within the collagen fibril. As we are unsure about the specific state the AGEs are within the ribose-treated collagen fibrils, we can only try to draw conclusions based upon the influence of AGEs on collagen fibril hydration. We expect the presence of AGE adducts to result in increase of collagen fibril swelling, and therefore reduced packing density. This is reflected by the decrease of indentation modulus in AFM and BLS measured longitudinal modulus. One limitation of our study to date is that we have not tested collagen fibrils in a tensile fashion. It may well be that under tension the changes upon AGE cross-linking would become more evident [56]. However, tension with *in situ* glycation is a complex experiment, beyond the scope of this study. Importantly, we show here that AGEs lead, at least in a first instance, to increased hydration, swelling and reduced transverse stiffness, which has not been reported before and underlines the need to better study the change in structure and mechanics of collagen fibrils upon exposure to increased levels of physiologically occurring and abundant sugars.

4. Conclusion

We tested the effect of sugar-mediated cross-links in collagen fibrils on their hydration and nanomechanical properties. To this end, Brillouin light scattering and atomic force microscopy experiments were performed. BLS clearly shows the effect of drying on the resulting spectra, with an increase in the longitudinal modulus as previously reported [33,34,36]. The BLS studies also show that while the transverse (perpendicular to fiber axis) properties differ significantly between the control and ribose treated fibers, the longitudinal (along fiber axis) properties remain similar and are less affected. Both however decrease with hydration, with the transverse properties more significantly. Here, the swelling was defined as the fold-increase in collagen fibril height upon hydration. Force-volume mapping additionally yielded measurements of indentation moduli at the individual collagen fibril level. Our results show that ribose-treated samples have a lower indentation modulus, which can be explained by their higher water content measured by AFM and is consistent with BLS measurements. Although, we cannot be sure at which state the AGEs are present in the collagen fibril we can draw conclusions based on hydration level and by comparison with other studies. Through this, we conclude that mostly AGE adducts are prevalent after 48 hours of treatment in ribose. Our study shows that BLS in combination with AFM can yield supportive evidence on the effect of AGEs in collagen fibrils on their hydration and their related mechanical properties. In the future, we aim to gain knowledge on the effect of AGEs have on collagen fibrils and through this provide a better understanding of the interplay between such cross-links, the hydration and nanomechanics.

Funding

European Cooperation in Science and Technology (CA16124); the University Library of Technische Universität Wien (Open Access Funding Programme); the Austrian Federal Ministry of Education, Science and Research; the Program Interreg VA-AT-CZ, project RIAT-CZ, No. ATCZ40, the Medical Research Council UK (G0900453), and the City of Vienna via the Vienna Business Agency.

Disclosures

The authors declare that there are no conflicts of interest related to this article.

Biomedical Optics EXPRESS

References

1. R. J. Johnson, M. S. Segal, Y. Sautin, T. Nakagawa, D. I. Feig, D.-H. Kang, M. S. Gersch, S. Benner, and L. G. Sánchez-Lozada, "Potential role of sugar (fructose) in the epidemic of hypertension, obesity and the metabolic syndrome, diabetes, kidney disease, and cardiovascular disease," Am. J. Clin. Nutr. **86**(4), 899–906 (2007).
2. K. S. Polonsky, "The past 200 years in diabetes," N. Engl. J. Med. **367**(14), 1332–1340 (2012).
3. A. J. Bailey, "Molecular mechanisms of ageing in connective tissues," Mech. Ageing Dev. **122**(7), 735–755 (2001).
4. A. J. Bailey, R. G. Paul, and L. Knott, "Mechanisms of maturation and ageing of collagen," Mech. Ageing Dev. **106**(1-2), 1–56 (1998).
5. K. L. Reigle, G. Di Lullo, K. R. Turner, J. A. Last, I. Chervoneva, D. E. Birk, J. L. Funderburgh, E. Elrod, M. W. Germann, C. Surber, R. D. Sanderson, and J. D. San Antonio, "Non-enzymatic glycation of type I collagen diminishes collagen-proteoglycan binding and weakens cell adhesion," J. Cell. Biochem. **104**(5), 1684–1698 (2008).
6. A. Bedi, A. J. Fox, P. E. Harris, X.-H. Deng, L. Ying, R. F. Warren, and S. A. Rodeo, "Diabetes mellitus impairs tendon-bone healing after rotator cuff repair," J. Shoulder Elbow Surg. **19**(7), 978–988 (2010).
7. V. M. Monnier, D. R. Sell, C. Strauch, W. Sun, J. M. Lachin, P. A. Cleary, and S. Genuth; DCCT Research Group, "The association between skin collagen glucosepane and past progression of microvascular and neuropathic complications in type 1 diabetes," J. Diabetes Complications **27**(2), 141–149 (2013).
8. A. W. Stitt, "Advanced glycation: an important pathological event in diabetic and age related ocular disease," Br. J. Ophthalmol. **85**(6), 746–753 (2001).
9. N. Sasaki, R. Fukatsu, K. Tsuzuki, Y. Hayashi, T. Yoshida, N. Fujii, T. Koike, I. Wakayama, R. Yanagihara, R. Garruto, N. Amano, and Z. Makita, "Advanced glycation end products in Alzheimer's disease and other neurodegenerative diseases," Am. J. Pathol. **153**(4), 1149–1155 (1998).
10. G. Basta, A. M. Schmidt, and R. De Caterina, "Advanced glycation end products and vascular inflammation: implications for accelerated atherosclerosis in diabetes," Cardiovasc. Res. **63**(4), 582–592 (2004).
11. A. M. Schmidt, S. D. Yan, J.-L. Wautier, and D. Stern, "Activation of receptor for advanced glycation end products: a mechanism for chronic vascular dysfunction in diabetic vasculopathy and atherosclerosis," Circ. Res. **84**(5), 489–497 (1999).
12. M. Saito and K. Marumo, "Collagen cross-links as a determinant of bone quality: a possible explanation for bone fragility in aging, osteoporosis, and diabetes mellitus," Osteoporos. Int. **21**(2), 195–214 (2010).
13. A. J. Fox, A. Bedi, X. H. Deng, L. Ying, P. E. Harris, R. F. Warren, and S. A. Rodeo, "Diabetes mellitus alters the mechanical properties of the native tendon in an experimental rat model," J. Orthop. Res. **29**(6), 880–885 (2011).
14. A. Galeski, J. Kastelic, E. Baer, and R. R. Kohn, "Mechanical and structural changes in rat tail tendon induced by alloxan diabetes and aging," J. Biomech. **10**(11/12), 775–782 (1977).
15. G. K. Reddy, "Cross-linking in collagen by nonenzymatic glycation increases the matrix stiffness in rabbit achilles tendon," Exp. Diabesity Res. **5**(2), 143–153 (2004).
16. G. K. Reddy, L. Stehno-Bittel, and C. S. Enwemeka, "Glycation-induced matrix stability in the rabbit achilles tendon," Arch. Biochem. Biophys. **399**(2), 174–180 (2002).
17. L. Maillard, "Action of amino acids on sugars. Formation of melanoidins in a methodical way," Compt. rend **154**, 66 (1912).
18. M. A. Karsdal, F. Genovese, E. A. Madsen, T. Manon-Jensen, and D. Schuppan, "Collagen and tissue turnover as a function of age: Implications for fibrosis," J. Hepatol. **64**(1), 103–109 (2016).
19. N. Verzijl, J. DeGroot, S. R. Thorpe, R. A. Bank, J. N. Shaw, T. J. Lyons, J. W. Bijlsma, F. P. Lafeber, J. W. Baynes, and J. M. TeKoppele, "Effect of collagen turnover on the accumulation of advanced glycation end products," J. Biol. Chem. **275**(50), 39027–39031 (2000).
20. D. R. Sell, K. M. Biemel, O. Reihl, M. O. Lederer, C. M. Strauch, and V. M. Monnier, "Glucosepane is a major protein cross-link of the senescent human extracellular matrix. Relationship with diabetes," J. Biol. Chem. **280**(13), 12310–12315 (2005).
21. V. R. Sherman, W. Yang, and M. A. Meyers, "The materials science of collagen," J. Mech. Behav. Biomed. Mater. **52**, 22–50 (2015).
22. B. Brodsky and A. V. Persikov, "Molecular structure of the collagen triple helix," Adv. Protein Chem. **70**, 301–339 (2005).
23. A. S. Craig, M. J. Birtles, J. F. Conway, and D. A. Parry, "An estimate of the mean length of collagen fibrils in rat tail-tendon as a function of age," Connect. Tissue Res. **19**(1), 51–62 (1989).
24. K. L. Goh, D. F. Holmes, H.-Y. Lu, S. Richardson, K. E. Kadler, P. P. Purslow, and T. J. Wess, "Ageing changes in the tensile properties of tendons: influence of collagen fibril volume fraction," J. Biomech. Eng. **130**(2), 021011 (2008).
25. O. G. Andriotis, S. W. Chang, M. Vanleene, P. H. Howarth, D. E. Davies, S. J. Shefelbine, M. J. Buehler, and P. J. Thurner, "Structure-mechanics relationships of collagen fibrils in the osteogenesis imperfecta mouse model," J. R. Soc. Interface **12**(111), 20150701 (2015).
26. O. G. Andriotis, S. Desissaire, and P. J. Thurner, "Collagen Fibrils: Nature's Highly Tunable Nonlinear Springs," ACS Nano **12**(4), 3671–3680 (2018).

Biomedical Optics EXPRESS

27. O. G. Andriotis, W. Manuyakorn, J. Zekonyte, O. L. Katsamenis, S. Fabri, P. H. Howarth, D. E. Davies, and P. J. Thurner, "Nanomechanical assessment of human and murine collagen fibrils via atomic force microscopy cantilever-based nanoindentation," J. Mech. Behav. Biomed. Mater. **39**, 9–26 (2014).
28. C. A. Grant, D. J. Brockwell, S. E. Radford, and N. H. Thomson, "Effects of hydration on the mechanical response of individual collagen fibrils," Appl. Phys. Lett. **92**(23), 233902 (2008).
29. C. A. Grant, D. J. Brockwell, S. E. Radford, and N. H. Thomson, "Tuning the elastic modulus of hydrated collagen fibrils," Biophys. J. **97**(11), 2985–2992 (2009).
30. A. J. Heim, T. J. Koob, and W. G. Matthews, "Low strain nanomechanics of collagen fibrils," Biomacromolecules **8**(11), 3298–3301 (2007).
31. A. J. Heim, W. G. Matthews, and T. J. Koob, "Determination of the elastic modulus of native collagen fibrils via radial indentation," Appl. Phys. Lett. **89**(18), 181902 (2006).
32. G. Scarcelli, W. J. Polacheck, H. T. Nia, K. Patel, A. J. Grodzinsky, R. D. Kamm, and S. H. Yun, "Noncontact three-dimensional mapping of intracellular hydromechanical properties by Brillouin microscopy," Nat. Methods **12**(12), 1132–1134 (2015).
33. F. Palombo, C. P. Winlove, R. S. Edginton, E. Green, N. Stone, S. Caponi, M. Madami, and D. Fioretto, "Biomechanics of fibrous proteins of the extracellular matrix studied by Brillouin scattering," J. R. Soc. Interface **11**(101), 20140739 (2014).
34. S. Cusack and S. Lees, "Variation of longitudinal acoustic velocity at gigahertz frequencies with water content in rat-tail tendon fibers," Biopolymers **23**(2), 337–351 (1984).
35. S. Cusack and A. Miller, "Determination of the elastic constants of collagen by Brillouin light scattering," J. Mol. Biol. **135**(1), 39–51 (1979).
36. R. Harley, D. James, A. Miller, and J. W. White, "Phonons and the elastic moduli of collagen and muscle," Nature **267**(5608), 285–287 (1977).
37. G. Scarcelli, P. Kim, and S. H. Yun, "In vivo measurement of age-related stiffening in the crystalline lens by Brillouin optical microscopy," Biophys. J. **101**(6), 1539–1545 (2011).
38. A. Masic, L. Bertinetti, R. Schuetz, S.-W. Chang, T. H. Metzger, M. J. Buehler, and P. Fratzl, "Osmotic pressure induced tensile forces in tendon collagen," Nat. Commun. **6**(1), 5942 (2015).
39. J. L. Hutter and J. Bechhoefer, "Calibration of atomic□force microscope tips," Rev. Sci. Instrum. **64**(7), 1868–1873 (1993).
40. W. F. Heinz and J. H. Hoh, "Spatially resolved force spectroscopy of biological surfaces using the atomic force microscope," Trends Biotechnol. **17**(4), 143–150 (1999).
41. W. C. Oliver and G. M. Pharr, "Measurement of hardness and elastic modulus by instrumented indentation: Advances in understanding and refinements to methodology," J. Mater. Res. **19**(01), 3–20 (2004).
42. D. J. Keller and F. S. Franke, "Envelope reconstruction of probe microscope images," Surf. Sci. **294**(3), 409–419 (1993).
43. B. P. Berne, R, *Dynamic Light Scattering with Applications to Chemistry, Biology and Physics* (Dover Publications, 2000).
44. R. Prevedel, A. Diz-Muñoz, G. Ruocco, and G. Antonacci, "Brillouin microscopy-a revolutionary tool for mechanobiology?" arXiv preprint arXiv:1901.02006 (2019).
45. F. Palombo and D. Fioretto, "Brillouin Light Scattering: Applications in Biomedical Sciences," arXiv preprint arXiv:1901.05176 (2019).
46. G. Scarcelli and S. H. Yun, "Confocal Brillouin microscopy for three-dimensional mechanical imaging," Nat. Photonics **2**(1), 39–43 (2007).
47. K. Elsayad, S. Werner, M. Gallemí, J. Kong, E. R. Sánchez Guajardo, L. Zhang, Y. Jaillais, T. Greb, and Y. Belkhadir, "Mapping the subcellular mechanical properties of live cells in tissues with fluorescence emission-Brillouin imaging," Sci. Signal. **9**(435), rs5 (2016).
48. S. Mattana, S. Caponi, F. Tamagnini, D. Fioretto, and F. Palombo, "Viscoelasticity of amyloid plaques in transgenic mouse brain studied by Brillouin microspectroscopy and correlative Raman analysis," J. Innov. Opt. Health Sci. **10**(6), 1742001 (2017).
49. J. Bella, M. Eaton, B. Brodsky, and H. M. Berman, "Crystal and molecular structure of a collagen-like peptide at 1.9 A resolution," Science **266**(5182), 75–81 (1994).
50. R. Z. Kramer, J. Bella, P. Mayville, B. Brodsky, and H. M. Berman, "Sequence dependent conformational variations of collagen triple-helical structure," Nat. Struct. Biol. **6**(5), 454–457 (1999).
51. S. Kudo, H. Ogawa, E. Yamakita, S. Watanabe, T. Suzuki, and S. Nakashima, "Adsorption of Water to Collagen as Studied Using Infrared (IR) Microspectroscopy Combined with Relative Humidity Control System and Quartz Crystal Microbalance," Appl. Spectrosc. **71**(7), 1621–1632 (2017).
52. G. D. Fullerton and A. Rahal, "Collagen structure: the molecular source of the tendon magic angle effect," J. Magn. Reson. Imaging **25**(2), 345–361 (2007).
53. A. Miller and J. S. Wray, "Molecular packing in collagen," Nature **230**(5294), 437–439 (1971).
54. R. I. Price, S. Lees, and D. A. Kirschner, "X-ray diffraction analysis of tendon collagen at ambient and cryogenic temperatures: role of hydration," Int. J. Biol. Macromol. **20**(1), 23–33 (1997).
55. M. P. E. Wenger, L. Bozec, M. A. Horton, and P. Mesquida, "Mechanical properties of collagen fibrils," Biophys. J. **93**(4), 1255–1263 (2007).
56. R. B. Svensson, S. T. Smith, P. J. Moyer, and S. P. Magnusson, "Effects of maturation and advanced glycation on tensile mechanics of collagen fibrils from rat tail and Achilles tendons," Acta Biomater. **70**, 270–280 (2018).